Simulation of Aerodynamic Entrainment Process of Soil Crust Based on Discrete Element Method

Wentao Hu[1,2], Zhengshi Wang[3], and Shuming Jia[1,2(✉)]

[1] College of Soil and Water Conservation Science and Engineering, Northwest A&F University, Yangling 712100, Shaanxi, China
{huwt,jiashm2020}@nwafu.edu.cn

[2] State Key Laboratory of Soil Erosion and Dryland Farming On the Loess Plateau, Institute of Soil and Water Conservation, Northwest A&F University, Yangling 712100, Shaanxi, China

[3] College of Natural Resources and Environment, Northwest A&F University, Yangling 712100, Shaanxi, China
wangzs2020@nwafu.edu.cn

Abstract. Wind erosion is one of the main causes of dust storms and land desertification in arid and semi-arid areas, and the existence of soil crust significantly increases resistance to wind erosion. However, the aerodynamic entrainment mechanism of crusted soil, a typical continuous-discrete coupled system, requires further investigation. In this study, the discrete sand particles and the continuous soil crust characterized by the spring damping model combined with the parallel bonding model were established in discrete element method (DEM). And the effects of crust thickness and strength on aerodynamic entrainment were studied. Simulation results showed that in comparison to the discrete sand, soil crust increased the threshold friction velocity to a factor of two to seven. The linear increase of particle take-off velocity and take-off angle with friction velocity was unaffected, and the thickness of the crust did not affect the distribution law of take-off velocity, or angle, but it did lower the take-off angle of the particles by about fifty percent. These results provided new insights into the mechanisms underlying the effects of crust on wind erosion.

Keywords: Soil Crust · Discrete Element Method (DEM) · Aerodynamic Entrainment

1 Introduction

The wind-blown sand movement is an important process that affects sediment transport, landform evolution, and climate change on Earth, Mars, and other terrestrial planets [1, 2]. As the first stage of the aeolian transport, the aerodynamic entrainment directly determines the threshold of sand particle motion and its subsequent development, and it also plays a crucial role in the unsaturated wind-sand flows [3, 4]. In arid and semi-arid regions, the soil crust was a key factor in reducing wind erosion and was more valuable than other factors [5].

X. Zheng and S. Balachandar (Eds.): IUTAM 2023, IUTAM Bookseries 41, pp. 178–187, 2024.
https://doi.org/10.1007/978-3-031-47258-9_11

Soil physical crust is a compact structure formed on the soil surface by non-biological processes such as raindrop splash and runoff erosion [6]. As a network of interconnected particle groups, the soil crust provides physical shields for soil particles, resisting the abrasion of the salting grains [7]. The rate of wind erosion on non-crusted surfaces was six to forty times that of crusted surfaces [7, 8]. As for the mechanism of aerodynamic entrainment, Anderson and Haff proposed a linear scaling law for aerodynamic entrainment based on momentum conservation, which has been extensively utilized in simulations of wind-blown sand movement [9]. Jia and Wang proposed a complete scheme for aerodynamic entrainment based on the discrete element method (DEM), and discovered that the cohesion force of particles increased the threshold friction velocity of aerodynamic entrainment, while almost not affecting the distribution of take-off angles and velocities [10].

Previous numerical simulations of aerodynamic entrainment have investigated the sand particle, but only a few on the continuum of the soil crust, which was commonly found in arid and semi-arid regions. Furthermore, the aerodynamic entrainment of the crust particle in a continuous-discrete coupled system (i.e., crust-sand) has not been studied. Although DEM simulations on the formation of the physical crust have been provided [11], additional research is required to determine how crust properties affect aerodynamic entrainment of particles.

Therefore, this study firstly introduces a parallel bonding model characterizing the continuum of crust and combines it with a spring damping model characterizing the discrete of sand. Secondly, a continuous-discrete coupled model of crust-sand sediment bed is developed. Thirdly, this study examines the evolution of particle diameter as a function of threshold friction velocity and the response time of aerodynamic entrainment under crusted conditions. Finally, the effects of crust strength and thickness on the aerodynamic entrainment of the crust particle are investigated.

2 Model and Method

2.1 Discrete Element Method of Particle Motion

The simulation was performed with the Discrete Element Method (DEM) developed by Cundall and Strack [12]. The governing equations of particle motion in DEM simulation are Newton's second laws, and the equations of translation and rotation are as follows

$$m\frac{dv_p}{dt} = F_c + F_d + mg \tag{1}$$

$$I\frac{d\omega_p}{dt} = M_c + M_d \tag{2}$$

where m and I stand for the particle mass and moment of inertia, v_p and ω_p are the particle velocity and angular velocity, respectively, $F_c = \sum_{i=1}^{n} F_{p_i}$ is the resultant contact force of all normal and frictional contacts, F_d means the fluid drag force, g denotes the gravitational acceleration, M_c and M_d indicate the contact and applied external moments acting on the particle, respectively.

2.2 Fluid Drag Force Model

For particles with no exposed area, the corresponding fluid drag force is zero, whereas for the exposed particles [13], the fluid drag force F_D is

$$F_D = m\frac{V_r}{T_p}f(\mathrm{Re}_p) \tag{3}$$

where $T_p = \rho_p d_p^2/(18\rho_f \nu) \sim 1.0e-2$ is the relaxation time [10], ρ_f and ν stand for the density and kinetic viscosity of air, respectively, $V_r = v_f - v_p$ means the relative velocity of the fluid and particle, $f(\mathrm{Re}_p)$ indicates a function related to the Reynolds number calculated as follows [14]

$$f(\mathrm{Re}_p) = \begin{cases} 1 & (\mathrm{Re}_p < 1) \\ 1 + 0.15\mathrm{Re}_p^{0.687} & (\mathrm{Re}_p \geq 1) \end{cases} \tag{4}$$

where $\mathrm{Re}_p = d_p V_r/\nu$ is the Reynolds number.

2.3 Dimensionless Parameters of Crust Strength and Thickness

The crust in the model was consistent with the structural crust described by Valentin and Bresson [6]. Compared to the biological crust, the structural crust has a simpler structure. Due to the lack of consistency in measuring crust properties, the following dimensionless parameters were proposed to characterize the crust strength and thickness

$$CS = F_\phi/G \tag{5}$$

$$CT = H/\mathrm{D} \tag{6}$$

where CS is the dimensionless crust strength, F_ϕ means the cohesions between crust particles, G stands for the gravitational force of the crust particle, CT is the dimensionless crust thickness, H indicates the vertical thickness of the crust, D means the diameter of the crust particle.

Field observations demonstrated that the thickness of the structural crust ranged from 1000 to 3000 μm, and wind tunnel experiments conducted by Sharratt and Vaddella revealed that some crusts thicker than two millimeters did not reach the threshold friction velocities [15]. Therefore, in this study, it was assumed that the crust thickness corresponded to two to ten times the diameter of the crust particles, i.e., a range of 400 to 2,000 μm under realistic conditions.

2.4 Discrete-Continuum Coupled Model for Sand-Crust Particles

A. **The parallel bonding model for characterizing the crust**

In this study, the cohesion force of the crust particles was characterized by the parallel bonding model [16], which was also commonly used in other cohesive particles such as ice [17] and snow [18]. The cohesion force was described with the following equations

$$\sigma = -\frac{F_n}{A} + |T|\frac{r_b}{L} \tag{7}$$

$$\tau = -\frac{F_s}{A} \tag{8}$$

where F_n and F_s are normal force and shear force, respectively, r_b means the bond radius, $A = \pi r_b^2$ indicates the bond area, T stands for the bending moment, $L = \pi r_b^4/4$ denotes the moment of inertia. If the normal or tensile stress exceeds the normal or tensile strength, the bond breaks and both F_n and F_s are set to zero, but the contact forces are not altered.

B. **The spring damping model for characterizing sand particles**

The sand particles were characterized by the spring damping model [12], with the following equations

$$F_n = \begin{cases} k_n \times \Delta\delta_n - \beta_n \times v & \Delta\delta_n \geq 0 \\ 0 & \Delta\delta_n < 0 \end{cases} \tag{9}$$

$$F_s = \begin{cases} k_s \times \Delta\delta_s - \beta_s \times r & F_s \leq \mu F_n \\ \mu \times F_n & F_s > \mu F_n \end{cases} \tag{10}$$

where F_n and F_s are normal force and shear force, $\Delta\delta_n$ and $\Delta\delta_s$ stand for normal and shear overlap of particles, β_n and β_s indicate normal and shear viscous damping ratio, respectively, v and r denote the normal relative velocity and shear relative deformation rate, respectively, μ means the frictional coefficient.

2.5 Wind Profile

The wind profile (Fig. 1) is applied through a standard logarithmic law [3]

$$u_x = \frac{u_*}{\kappa}\ln(\frac{z}{z_0}) \tag{11}$$

where u_* is the fluid shear velocity, $\kappa = 0.4$ is the Karman constant, z stands for the altitude above the bed surface, $z_0 = d_p/30$ means the aerodynamic roughness [1].

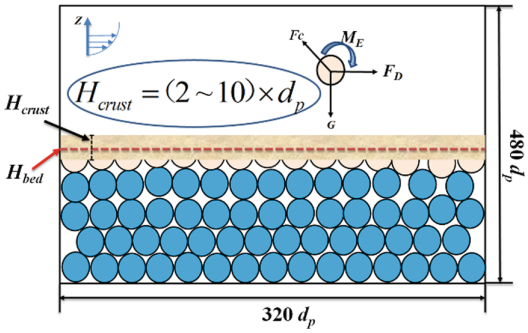

Fig. 1. Schematic diagram for determination of the bed height, crust thickness and forces applied on the airborne crust particle ($d_p = 200$ μm)

2.6 Simulation Procedures and Model Settings

The numerical simulation domain was set as $L_x \times L_y = 320\,d_p \times 480\,d_p$. The top and bottom boundaries were set reflective conditions, and the left and right boundaries were set periodic conditions. Simulation procedures are as follows.

1. A amount of 8000 particles were randomly generated within the domain to form a sediment bed. The criterion for the calm bed was $V_{p\max} \leq 1.0e-4$ m/s.
2. The particles above H_0 ($H_0 = 12d_p$) were removed to form a flat sediment bed. Three repetitions of the above step ensured a calm and steady state. The porosity of the bed was approximately 0.5. The bed height $H_{bed} = H_0 - pd_p$ at which the mean wind velocity reduced to zero was determined (Fig. 1).

After generation, particles were divided into two groups including crust and sand, and different physical properties and contact models (Table 1), were set to characterize the continuum and the discrete type. The force chain network of the coupled model was shown in Fig. 2.

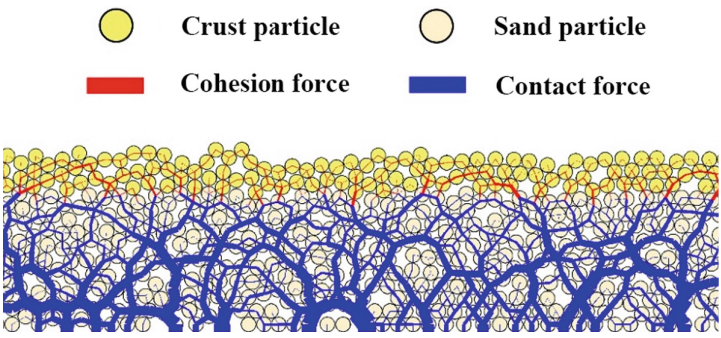

Fig. 2. Distributions of cohesion forces and contact forces in force chain network formed by the discrete-continuum coupled model

Table 1. Parameters used in DEM simulation

Parameter	Description	Value	Unit
k_n	Normal stiffness	2e6	Nm^{-1}
k_s	Shear stiffness	2e6	Nm^{-1}
μ	Frictional coefficient	0.30	–
σ_c	Normal bonding strength	4e4–5e4	Pa
τ_c	Shear bonding strength	4e4–5e4	Pa
ρ_p	Particle density	2650	kgm^{-3}
d_p	Particle diameter	200	μm
ρ_f	Air density	1.225	kgm^{-3}
v	Kinematic viscosity of air	1.5e-5	ms^{-2}
βn	Normal viscous damping ratio	0.2	–
βs	Shear viscous damping ratio	0.2	–
E	Young's modulus	1e6	Nm^{-2}

3 Results and Discussion

3.1 Model Validation

The threshold friction velocity determines the subsequent movement of particles. As shown in Fig. 3a, the linear scaling law between the particle diameter and the threshold friction velocity were verified, compared to the existing simulation result. In addition, three groups of field experiments under crusted conditions were included.

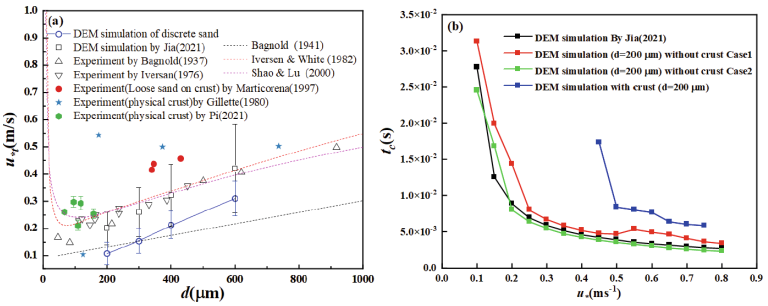

Fig. 3. **a.** Comparisons of simulated and measured threshold velocities $u*_t$ as a function of particle diameter d; and **b** validations of response time t_c as a function of threshold velocities $u*_t$ under sand and crusted conditions compared to Jia [10]

The response time of the first lifting particle was also investigated under crusted conditions. As shown in Fig. 3b, with the inter-particle cohesions, the exponential decline law between response time and friction velocity under crusted conditions was consistent with those in sand cases.

3.2 Influences of Crust Strength and Crust Thickness on the Threshold Aerodynamic Friction Velocity

Under the condition of no inter-particle cohesions, the threshold friction velocity of sand particles ($d_p = 200$ μm) was approximately 0.1 m/s, as shown in Fig. 4. The threshold friction velocity increased by approximately two to seven times under crusted conditions, and the threshold friction velocity increased linearly with crust strength and thickness. However, once the crust thickness reached the critical value of 5 D, the threshold friction velocity nearly remained constant as the crust thickness increased.

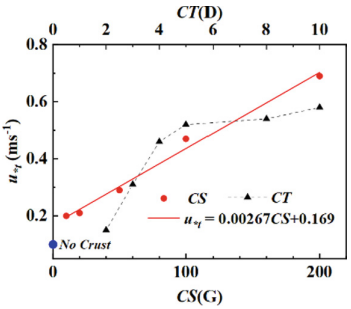

Fig. 4. Crust strength (CS) and Crust thickness (CT) as functions of threshold velocities u_{*t}. The red line is the linear regression equation of crust strength F_Φ versus threshold velocities u_{*t}, and the dash line with scatter for crust thickness H versus threshold velocities u_{*t}

Since the fluid drag force was related to the friction velocity, the linear increase between threshold friction velocity and crust strength could be explained by the larger fluid drag force required to brake the parallel bonds.

This phenomenon occurred because the distance between crust particles was constrained by the inter-particle cohesion force. Within a certain range, crust particles from the lower layer had a "delaying" effect on the aerodynamic entrainment of crust particles from the upper layer. However, beyond a certain range, this "delaying" effect was only manifested by the influence of particles in the upper layer and was independent of crust thickness.

3.3 Distributions of Take-Off Velocity and Angle Under Different Crust Strength and Crust Thickness

Here, the particle take-off velocity is defined as $\mu_p = \sqrt{\mu_u^2 + \mu_w^2}$, where μ_p is the particle velocity, decomposed into the streamwise velocity (μ_u) and vertical velocity (μ_w) along the X-axis and Y-axis, respectively. The particle velocity was obtained directly from the program output.

The streamwise and vertical velocities of particle take-off exhibited a consistent linear scaling law in the absence of cohesions. As shown in Fig. 5a and 5b, the linear scaling law of take-off velocity with the friction velocity still remained when the crust strength reached 100 G and 200 G, which was consistent with the simulation results

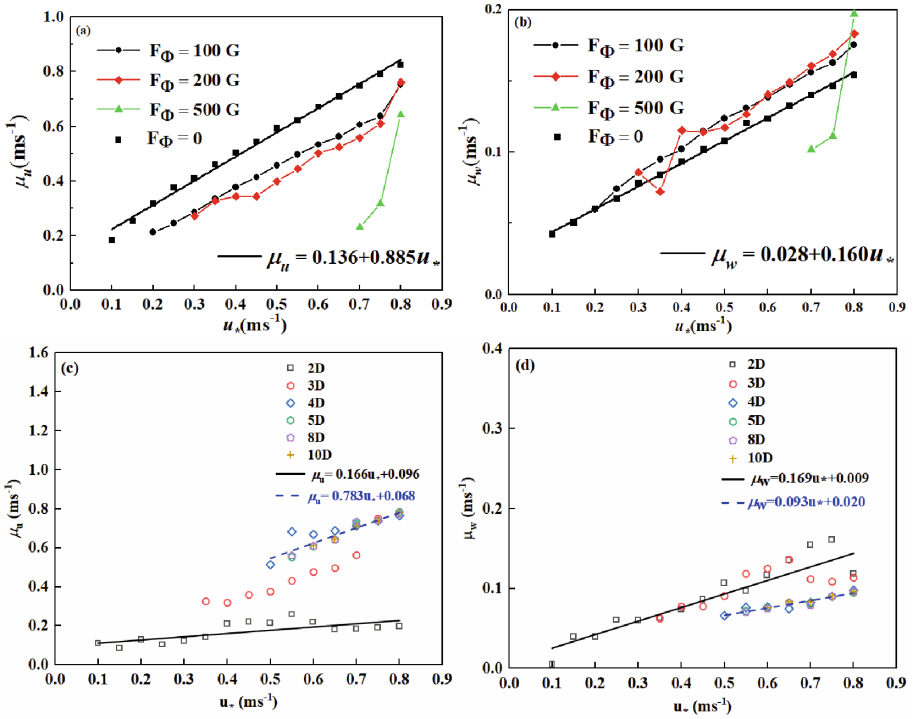

Fig. 5. Evolutions of streamwise velocities μ_u and vertical velocities μ_w versus the friction velocity $u*$ under different crust strengths F_Φ for **a** and **b**, respectively; and crust thicknesses H for **c** and **d**. The data of H = 2 D, 5 D, 8 D and 10 D are calculated in linear regression

of Jia and Wang [10]. When the crust strength exceeded 200 G, the take-off velocity changed from a linear scaling law to an exponential scaling law, and this relationship was significant at 500 G.

When the crust thickness exceeded 5 D, the take-off velocity remained almost unchanged with the increase of crust thickness. The critical value of the crust thickness affecting take-off velocity was between 4 D and 5 D. The take-off velocity and angle reflected the first lifting particle kinetic energy, and the aerodynamic entrainment process converted fluid kinetic energy into particle kinetic energy. The inter-particle cohesions just postponed this conversion process without affecting the linear scaling law, whereas the excessive cohesions prevented particles from accumulating energy from sliding and collision processes of the aerodynamic entrainment.

The particle take-off angle is defined as $\alpha_u = \arctan(\mu_w/\mu_u)$, where μ_w is the vertical velocity and μ_u is the streamwise velocity.

Figure 6 presented the take-off angle α_u as a function of friction velocities $u*$ under conditions of sand and crust thicknesses. It can be found that the take-off angle α_u was roughly distributed between 12° and 13° without F_Φ, and the maximum take-off angle at various $u*$ increased from roughly 15° to 26° with the increase of F_Φ.

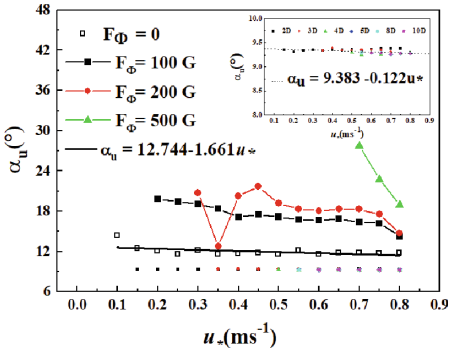

Fig. 6. Take-off angle α_u as a function of friction velocities $u*$ under conditions of sand and crust thicknesses H

Seen from Fig. 6, the take-off angle α_u remained basically constant with the increase of crust thickness H, roughly distributed in the range of 9.2° to 9.4°. When H exceeded 5 D, the evolution of the α_u with $u*$ remained relatively stable. In this case, the $u*$ did not affect the α_u under thicker crusted conditions.

4 Conclusions

Combining the parallel bonding model and the spring damping model, this study presents a coupled continuous-discrete model of crust-sand sediment bed, and investigates the effects of crust strength and thickness on the aerodynamic entrainment process. The study reveals that the crust strength delays the response time and increases the threshold friction velocity of aerodynamic entrainment to about two to seven times compared to non-crusted conditions, but it does not change distribution laws of particle take-off velocity and angle with the friction velocity. A critical value of five times of crust thicknesses is determined and the take-off angle under crusted conditions is approximately fifty percent smaller than that of non-crusted conditions. The fluid drag force, inter-particle cohesions and the gravity determine the aerodynamic entrainment, and the crust exhibits obstructive and delaying characteristics in the process.

This study proposes a comprehensive aerodynamic entrainment scheme for sand particles under crusted conditions, providing more accurate predictions for sandstorms and desertification, and offers an insight into the optimization of desertification control measures.

Acknowledgements. This work was supported by the National Natural Science Foundation of China (11902341, 12102364), the China Postdoctoral Science Foundation (2021M702679), the Young Talent Fund of University Association for Science and Technology in Shaanxi, China (20210503), and the Chinese Universities Scientific Fund (2452021048, 2452020266).

References

1. Bagnold, R.A.: The Physics of Blown Sand and Desert Dunes. Methuen, London (1942)

2. Kok, J.F., Parteli, E.J., Michaels, T.I., Karam, D.B.: The physics of wind-blown sand and dust. Rep. Prog. Phys. Phys. Soc. **75**, 106901 (2012)
3. Shao, Y.: Physics and Modelling of wind Erosion. Springer, Newyork (2008). https://doi.org/10.1007/978-1-4020-8895-7_9
4. Li, G., Zhang, J., Herrmann, H.J., Shao, Y., Huang, N.: Study of aerodynamic grain entrainment in aeolian transport. Geophys. Res. Lett. **47**, e2019GL086574 (2020)
5. Hagen, L., Zobeck, T., Skidmore, E., Elminyawi, I.: WEPS technical documentation: soil submodel. In: SWCS WEPP/WEPS Symposium, Ankeny, IA, pp. 9–11. Soil and Water Conservation Society, Ankeny (1995)
6. Valentin, C., Bresson, L.-M.: Morphology, genesis and classification of surface crusts in loamy and sandy soils. Geoderma **55**, 225–245 (1992)
7. Chepil, W.S.: Soil Conditions that Influence Wind Erosion. USDA-ARS Tech. Bull, Washington, DC (1958)
8. Zobeck, T.M.: Soil properties affecting wind erosion. J. Soil Water Conserv. **46**, 112–118 (1991)
9. Anderson, R.S., Haff, P.K.: Simulation of eolian saltation. Science **241**, 820–823 (1988)
10. Jia, S., Wang, Z.: Simulation of aerodynamic entrainment with interparticle cohesions based on discrete element method. Earth. Surf. Proc. Land. **46**, 1410–1418 (2021)
11. Yeom, S., Sjoblom, K.: Structural soil crust development from raindrop impacts using two-dimensional discrete element method. Comput. Geosci. **97**, 49–57 (2016)
12. Cundall, P.A., Strack, O.D.: A discrete numerical model for granular assemblies. Geotechnique **29**, 47–65 (1979)
13. Dey, S., Papanicolaou, A.: Sediment threshold under stream flow: a state-of-the-art review. KSCE J. Civ. Eng. **12**, 45–60 (2008)
14. Clift, R., Grace, J.R., Weber, M.E.: Bubbles, Drops, and Particles. Dover Publications, Newyork (2005)
15. Sharratt, B., Vaddella, V.: Threshold friction velocity of crusted windblown soils in the Columbia Plateau. Aeol. Res. **15**, 227–234 (2014)
16. André, D., Iordanoff, I., Charles, J.-L., Néauport, J.: Discrete element method to simulate continuous material by using the cohesive beam model. Comput. Methods Appl. Mech. Eng. **213–216**, 113–125 (2012)
17. Long, X., Liu, L., Liu, S., Ji, S.: Discrete element analysis of high-pressure zones of sea ice on vertical structures. J. Mar. Sci. Eng. **9**(3), 348 (2021)
18. Comola, F., Kok, J.F., Gaume, J., Paterna, E., Lehning, M.: Fragmentation of wind-blown snow crystals. Geophys. Res. Lett. **44**(9), 4195–4203 (2017)